LASER INTERFEROMETER GRAVITATIONAL WAVE OBSERVATORY
- LIGO -
CALIFORNIA INSTITUTE OF TECHNOLOGY
MASSACHUSETTS INSTITUTE OF TECHNOLOGY

Technical Note	**LIGO-T2200177–**	2022/08/04

Fisher Information Analysis for Emissivity Estimation

Hiya Gada

California Institute of Technology
LIGO Project, MS 18-34
Pasadena, CA 91125
Phone (626) 395-2129
Fax (626) 304-9834
E-mail: info@ligo.caltech.edu

Massachusetts Institute of Technology
LIGO Project, Room NW22-295
Cambridge, MA 02139
Phone (617) 253-4824
Fax (617) 253-7014
E-mail: info@ligo.mit.edu

LIGO Hanford Observatory
Route 10, Mile Marker 2
Richland, WA 99352
Phone (509) 372-8106
Fax (509) 372-8137
E-mail: info@ligo.caltech.edu

LIGO Livingston Observatory
19100 LIGO Lane
Livingston, LA 70754
Phone (225) 686-3100
Fax (225) 686-7189
E-mail: info@ligo.caltech.edu

http://www.ligo.caltech.edu/

Contents

1 Introduction

The Laser Interferometer Gravitational-Wave Observatory (LIGO) measures gravitational waves and is one of the pioneering instruments which help detect black holes and neutron star mergers. The instrument, or more accurately, the suspended mirrors used, is highly susceptible to vibration noise. The third-generation upgrade, LIGO Voyager, is planned to improve the sensitivity by an additional factor of two and halve the low-frequency cutoff to 10 Hz by reducing quantum radiation pressure and shot noise, mirror thermal noise, mirror suspension thermal noise, and Newtonian gravity noise. The thermal vibrations (or thermal noise) are nullified by installing a cryogenic cooling facility which radiatively cools the silicon test masses to 123 K.

1.1 Background

Constancio et al. [1] theorized that the silicon test masses would require a high thermal emissivity coating to increase the radiative coupling to its cold environment and effectively dissipate the absorbed laser power. To this end, we wish to determine the emissivities of various black coatings as a function of temperature and subsequently use the best emissivity material for the Mariner (Voyager prototype) upgrade at the Caltech 40m Lab. This is done by obtaining cool-down curves in a cryostat designed specifically for the purpose of emissivity measurement. Using a simplified heat transfer model, the emissivity and corresponding propagated uncertainty is extracted from the cool-down temperature data.

1.2 Motivation

Running the experiment and obtaining the cool-down data is expensive and time-consuming, with a time constant of several days. It becomes infeasible to run the experiments multiple times and find the expected value of the emissivity. We thus run simulations prior to the experiment and find the optimal experimental configuration and excitation, which gives us emissivity with the least uncertainty, using Fisher Information Matrix analysis. The optimal configuration and excitation input obtained will then be used in the experiment to get a close to accurate measurement of emissivity.

The lab's ongoing work includes making design changes to the cryostat, which would minimize heat leaks into the system. It would allow the test mass to cool down to 123 K quickly and reduce the thermal noise injected into the system to get a less uncertain cool-down output. My project would complement this effort by theoretically determining which design parameters contribute the most to the uncertainty in emissivity and even suggest changes in their values for future design upgrades of the cryostat. It would also corroborate the design changes already made and recommend what optimal excitation should be given to make the system robust to noise. Further the same optimal experimental configuration and excitation obtained as a result of this project can be used for emissivity tests of many key coating materials for the LIGO Voyager upgrade.

2 The Cryostat

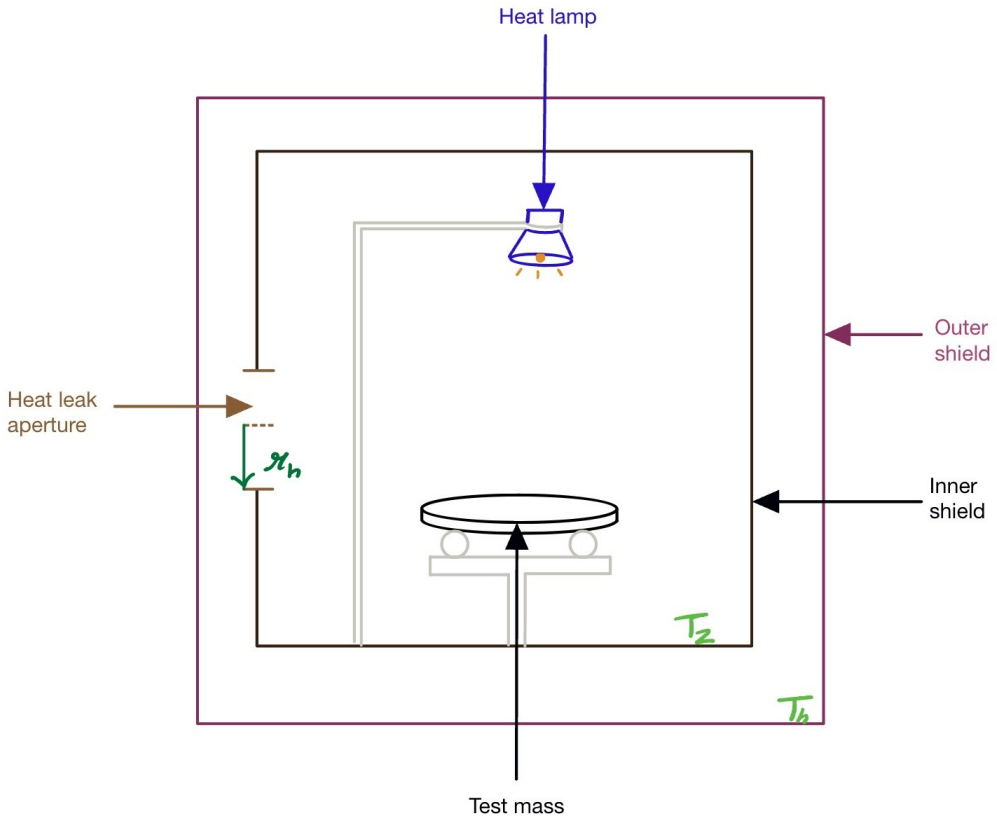

Figure 1: The cryostat

In our latest experiment, we use a thin wafer instead of a bulk mass because it is easier to mass produce wafers for numerous experiments at a low cost. A new mechanical setup (see figure 1) is designed to hold the wafer in place. We also add a heater (a heating lamp) to give the necessary optimal control input from our Fisher Matrix analysis. It is also useful to heat the set-up after an experiment back to room temperature.

The parameters of our experiment, especially the geometric view factor, is modified and used for further simulations. The notation used in the report is the same as that used in Interim Report 1.

3 Steady State Excitation

We modify the original experiment by applying a heat input in a particular interval when the components have reached steady state. We assume the other temperatures (T_2 and T_h) do not vary a lot during the excitation because of the system's huge time constant (hence, steady state).

We also introduce a new parameter called T_1° which will be the temperature of the test mass immediately after the excitation stops (see figure 2). This user-defined parameter allows us

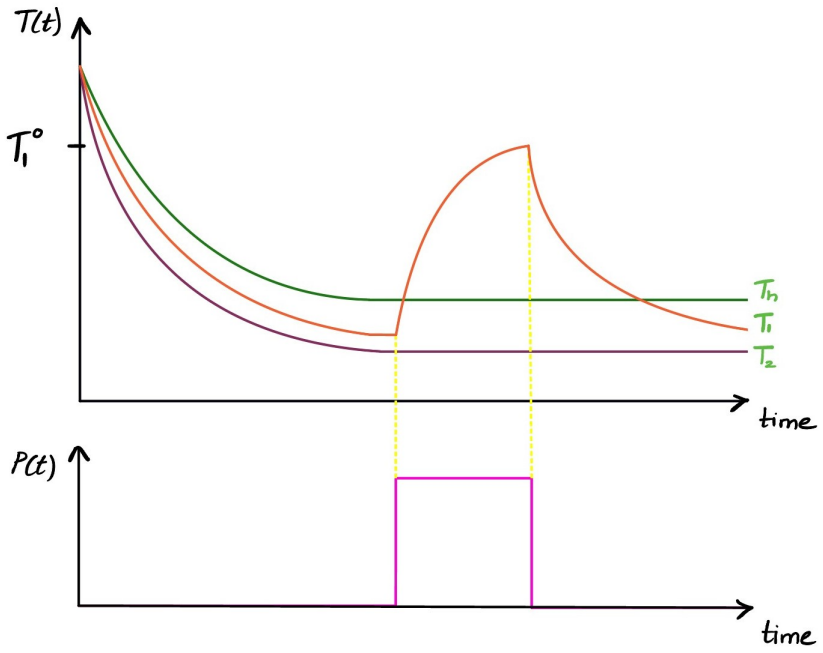

Figure 2: Rectangular excitation at steady state

to begin our analysis after the point $T_1 = T_1^\circ$ and conveniently ignore prior transient data. Thus, there is also no need to model the heat input as long as we reach the temperature T_1° fairly quickly. We can now analyse the cool down curve after the excitation assuming steady state T_2 and T_h.

3.1 Time Domain Analysis

The time domain analysis takes the output to be T_1 and the parameters as $\bar{\theta} = \{T_1^\circ, \epsilon_1\}$. The observations/measurements are taken at every time step, over which it is summed.

$$\mathcal{F}_{ij} = \sum_t \frac{1}{\sigma_T^2} \left(\frac{\partial T_1}{\partial \theta_i} \frac{\partial T_1}{\partial \theta_j} \right), \tag{1}$$

where σ_T is assumed to be a constant (constant excitation and noise). We get a 2×2 Fisher matrix which we invert to get the covariance matrix. The term corresponding to (ϵ_1, ϵ_1) is minimized over different T_1° and ϵ_1 values to find the optimal experimental configuration. No control input is considered as our analysis starts at $T_1 = T_1^\circ$.

3.2 Results

Numerically this is done by making a Fisher matrix grid, i.e., elements of a Fisher matrix are calculated at every combination of (T_1°, ϵ_1). A disadvantage of this method is that it is computationally intensive, but it is still explored as we don't have an explicit analytical function of the Fisher matrix to optimize.

Figure 3 shows the contour plot of the (ϵ_1, ϵ_1) term, the variance of ϵ_1, in the covariance matrix ($\mathcal{C} = \mathcal{F}^{-1}$).

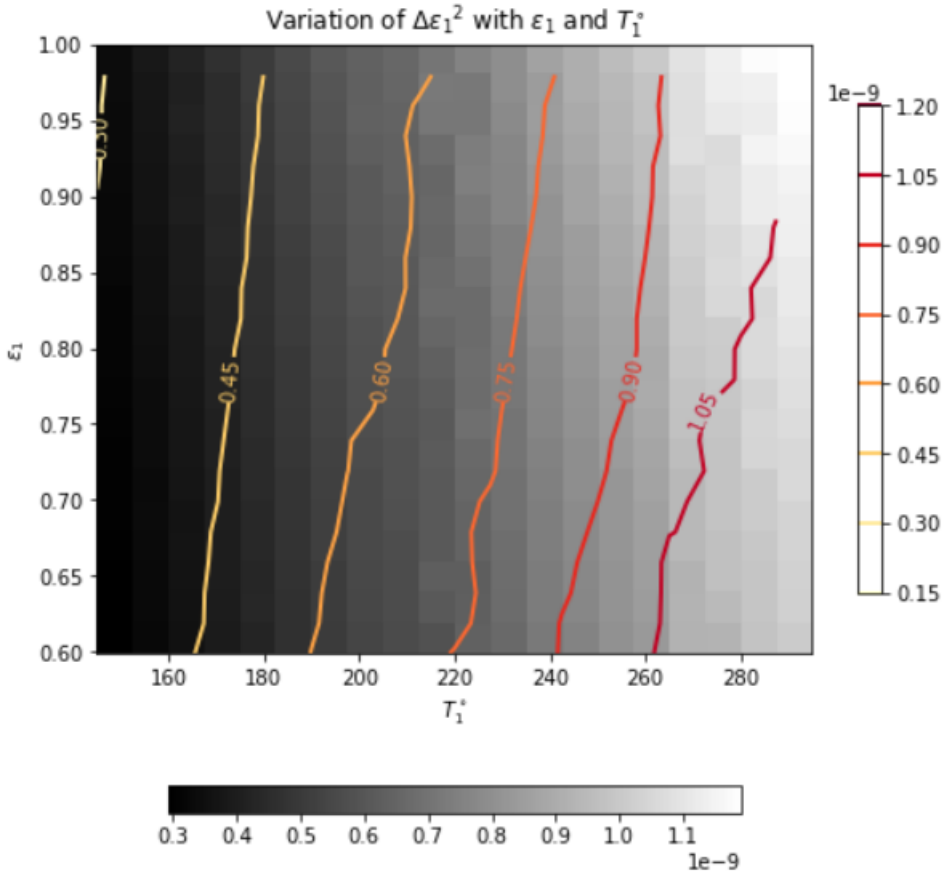

Figure 3: Variation of variance ϵ_1 for different combinations of ϵ_1 and T_1°

We see that for a particular value of ϵ_1, uncertainty increases with T_1° value. Thus, we want the lowest temperature T_1° possible. It shows the way in which we have set-up the experiment is not very useful, as the most ideal result is to not provide any heat excitation at all.

4 Time Domain Analysis of Linearized System

We linearize our system about the equilibrium test mass temperature as done in Interim Report 1,

$$\dot{T}_1(t) = AT_1(t) + Bu(t) \tag{2}$$

where, $u(t)$ is our heat input. The parameters are encapsulated in A. For our system $B = 1$. We solve for T_1 using Laplace transform,

$$\begin{aligned}
\mathcal{L}\{\dot{T_1}(t)\} &= \mathcal{L}\{AT_1(t) + Bu(t)\} \\
sT_1(s) - T_1^\circ - AT_1(s) &= BU(s), \\
T_1(s) &= \frac{BU(s)}{s-A} + \frac{T_1^\circ}{s-A}, \\
T_1(t) &= \mathcal{L}^{-1}\left\{\frac{BU(s)}{s-A}\right\} + T_1^\circ e^{At}.
\end{aligned}$$

We see the first term of the solution has the heat input along with the system parameter A. We can conclude that solving for the Fisher matrix, by differentiating T_1 by parameters $\{\theta_i\}$, will include the excitation terms parameters (amplitude and frequency of the input signal) as well. Thus, we were initially wrong about the control input not affecting the covariance matrix.

Time-domain analysis should indeed give us an optimal control input. The results would be the same as those obtained using frequency domain analysis, as we are analysing output of the same system, just in a different domain. For a linear system, solving the Fisher Matrix in the frequency domain becomes algebraic and therefore easier than solving in the time domain. Future work involves analysing this method particularly for the non-linear form of our system without assuming any steady state conditions.

5 Frequency Domain Analysis of Linearized System

[2] provides a framework for finding optimal excitation using Fisher Matrix for a two parameter system. We started out with finding one optimal frequency, as done in [2], and got a nonzero determinant for the Fisher Matrix. We also observed that the optimal frequency matched the time constant of our system (see Figure 4).

5.1 Optimal excitation

We first do an analysis for a two frequency system with the same standard deviation assigned to both the frequencies. Figure 4 shows how the determinant varies for different frequency values. We see that the optimal set of frequencies are degenerate and this is because we have given them the same or constant standard deviation (independent on frequency). This would mean that for white noise injected in the system, the excitation amplitudes of the frequencies are the same. We get non-degenerate optimal frequencies if we divide the total power between the two frequencies unequally. This tells us that that optimal input powers need to be considered alongside optimal frequencies.

5.2 Optimal experimental configuration

Using the optimal frequencies obtained in the previous analysis, we find the system parameters which maximize the determinant of the Fisher Matrix.

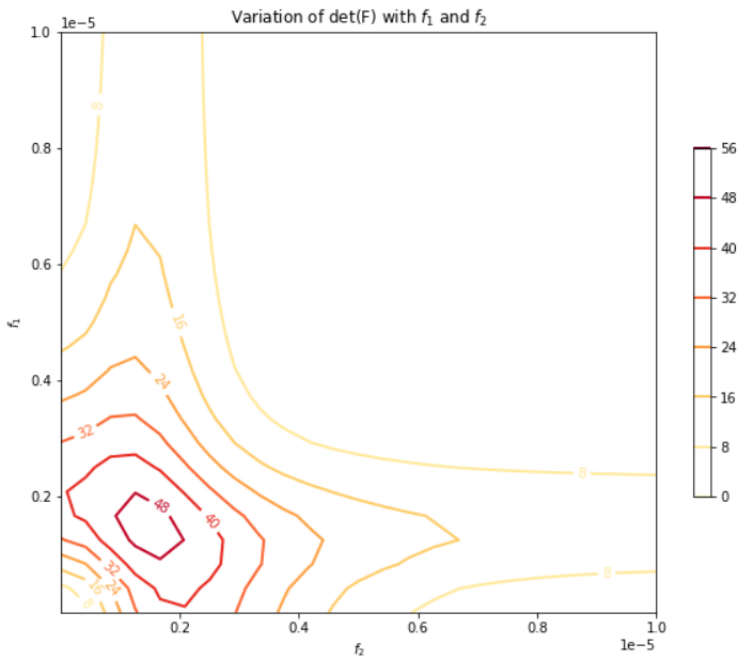

Figure 4: Variation of $det(F)$ with signal frequencies

Figure 5 shows that for a particular value of ϵ_1, we see that determinant is maximum at least value of ϵ_2. There is a trade-off between getting good radiative coupling by having a large ϵ_2 and a lesser uncertainty in ϵ_1 by having a small ϵ_2.

6 Power Spectrum Optimization

This method involves distributing some fixed total power among discrete frequencies within a particular range. Finding optimal frequencies by maximizing the determinant of the Fisher Matrix involves choosing the excitation amplitude of the signal beforehand (when assigning the standard deviation for that frequency). The power spectrum optimization algorithm introduced in [3] gives us information about what the optimum power distribution should be, It can be used constrain the total power and also find the optimal excitation amplitude for a range of frequencies. However, these results should still agree with our Fisher Matrix analysis.

6.1 Dispersion Function

Dispersion function $\nu(\chi, \Omega_k)$, as defined in [3], for a given input power spectrum $\chi(\Omega) = (|U(1)|^2, \cdots, |U(F)|^2)$, with $\sum_{k=1}^{F} |U(k)|^2 = \mathfrak{P}$ is,

$$\nu(\chi, \Omega_k) = \text{trace}([\mathcal{F}(\chi)]^{-1} fi(\Omega_k)),$$

with $\mathcal{F}(\chi)$ the information matrix resulting from the design $\chi(\Omega), fi(\Omega_k)$ the information matrix corresponding to a single frequency input with a normalized power spectrum $|U(k)|^2 = \mathfrak{P}$, and Ω_k the frequency.

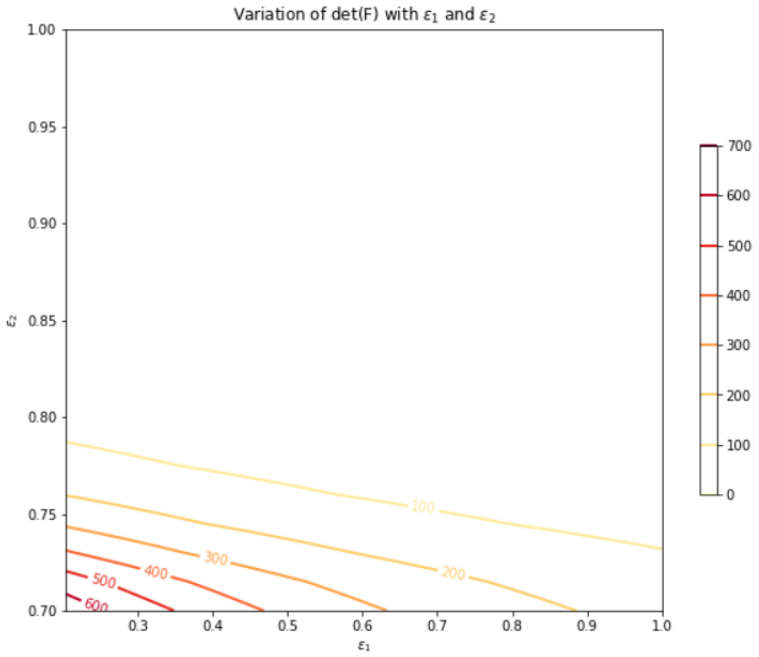

Figure 5: Variation of $det(F)$ for different ϵ_1 and ϵ_2

To intuitively understand the meaning of this function, we will look at the one parameter case. The dispersion function then can be explained as a scalar measure of the covariance for the given input power spectrum with respect to the covariance for a single frequency input with normalized (concentrated) power spectrum.

One of the properties of the dispersion function is that the maximum of the dispersion function over the frequency grid is larger than or equal to the number of parameters. Thus our aim is to minimize the dispersion function and make it converge to the number of parameters.

In a way it can be understood how bad the covariance of our system is, at the estimated parameters, in comparison to the covariance when the power is concentrated at one frequency. It encourages us to find a power distribution which minimizes the covariance instead of concentrating the power at one frequency (which may or may not be one of the optimal frequencies).

Another way of expressing the dispersion function, as done in [3],

$$\nu(\chi, \Omega_k) = \frac{2\sigma_G^2(\Omega_k, \bar{\theta})\mathfrak{P}}{\sigma_U^2(k)|G(\Omega_k)|^2 + \sigma_Y^2(k) - 2\,\mathrm{Re}(\sigma_{YU}^2(k)\bar{G}(\Omega_k))}.$$

This can be interpreted as the ratio of the variance of the system frequency response, calculated with the estimated parameters, to the noise power of the measurements at the frequency Ω_k.

This makes sense as we want to minimize the variance of the frequency response (which encodes the system parameters) with respect to a particular noise power.

6.2 Algorithm

- **Step 1:** Select a set of frequencies $\mathbb{F} = \{\Omega_1, \cdots, \Omega_F\}$ within our band of interest. The input power is distributed equally amongst these F frequencies (called design χ_0).
- **Step 2:** Set $i = i + 1$ in the numerical algorithm and calculate $\nu(\chi_i, \Omega_k)$ for $k = 1, \cdots, F$.
- **Step 3:** Let n_θ be the number of parameters. Compose new design,

$$\chi_{i+1}(\Omega_k) = \chi_i(\Omega_k) \frac{\nu(\chi_i, \Omega_k)}{n_\theta} \quad \text{for } k = 1, \cdots, F.$$

- **Step 4:** If $\max(\nu(\chi_i, \Omega_k) - n_\theta) < \epsilon$ with a sufficiently small ϵ and $\Omega_k \in \mathbb{F}$, then the optimal design is found. Otherwise, we return to Step 2.

6.3 Toy Problem

We use the example in [2] to verify our algorithm with the results in the paper. The transfer function is given as,

$$G(s) = \frac{k}{1 + \frac{s}{p}}$$

The total power is taken to be 1 kW and is initially distributed equally among 50 frequencies $\mathbb{F} = \{0, \cdots, p_{est}\}$ where $p_{est} = 350$ Hz is the initial estimate or prior on p. The prior on k is given by $k_{est} = 3.2$ mA/pm.

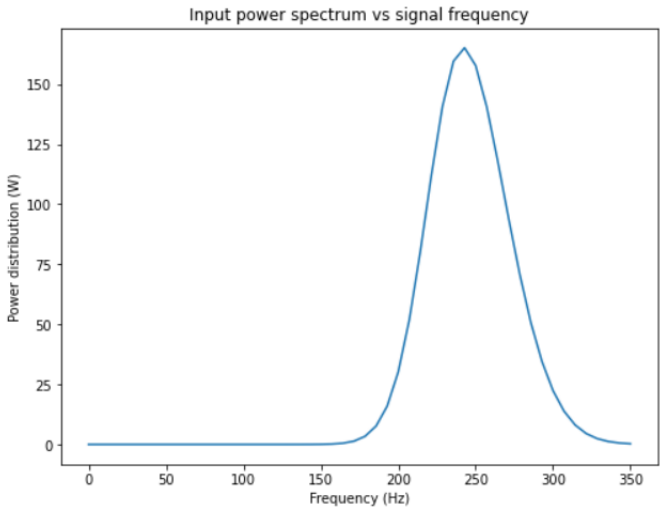

Figure 6: Power spectrum optimization

Figure 6 shows us how the power is distributed amongst various frequencies. We see the power is maximum at a particular optimal frequency value of 242.86 Hz. The Evan Hall analysis in [2] gives us the optimal frequencies as $p_{est}/\sqrt{3} = 202.07$ Hz and $p_{est}/2 = 247.48$ Hz to minimize the determinant and the (p, p) element of the covariance matrix, Σ, respectively.

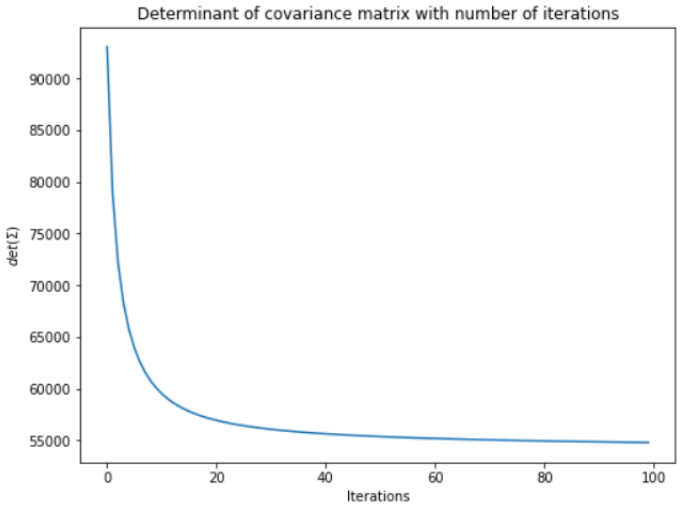

Figure 7: Variation of $det(\Sigma)$ with number of iterations

Thus the result we obtained using this algorithm is somewhere between the two minimization objectives we want.

Figure 7 shows us how the algorithm ensures minimization of $det(\Sigma)$ with each iteration. This meets our ultimate objective.

References

[1]M. Constancio Jr, R. X. Adhikari, O. D. Aguiar, K. Arai, A. Markowitz, M. A. Okada, and C. C. Wipf, "Silicon emissivity as a function of temperature", International Journal of Heat and Mass Transfer **157**, 119863 (2020).

[2]E. D. Hall, "Fisher matrix methods for transfer function measurement", ligo (2015).

[3]R. Pintelon and J. Schoukens, *System identification: a frequency domain approach* (John Wiley & Sons, 2012).

[4]J. Tellinghuisen, "Statistical error propagation", The Journal of Physical Chemistry A **105**, 3917–3921 (2001).

[5]D. Wittman, "Fisher matrix for beginners", Technical report, UC Davis.

[6]Y. A. Çengel, *Heat transfer: a practical approach*, McGraw-Hill series in mechanical engineering (McGraw-Hill, 2003) Chap. 12.

[7]R. X. Adhikari, K. Arai, A. F. Brooks, C. Wipf, O. Aguiar, P. Altin, B. Barr, L. Barsotti, R. Bassiri, A. Bell, G. Billingsley, R. Birney, D. Blair, E. Bonilla, J. Briggs, D. D. Brown, R. Byer, H. Cao, M. Constancio, S. Cooper, T. Corbitt, D. Coyne, A. Cumming, E. Daw, R. deRosa, G. Eddolls, J. Eichholz, M. Evans, M. Fejer, E. C. Ferreira, A. Freise, V. V. Frolov, S. Gras, A. Green, H. Grote, E. Gustafson, E. D. Hall, G. Hammond, J. Harms, G. Harry, K. Haughian, D. Heinert, M. Heintze, F. Hellman, J. Hennig, M. Hennig, S. Hild, J. Hough, W. Johnson, B. Kamai, D. Kapasi, K. Komori, D. Koptsov, M. Korobko, W. Z. Korth, K. Kuns, B. Lantz, S. Leavey, F. Magana-Sandoval, G. Mansell, A. Markosyan, A. Markowitz, I. Martin, R. Martin, D. Martynov, D. E. McClelland, G. McGhee, T. McRae, J. Mills, V. Mitrofanov, M. Molina-Ruiz, C. Mow-Lowry, J. Munch, P. Murray, S. Ng, M. A. Okada, D. J. Ottaway, L. Prokhorov, V. Quetschke, S. Reid, D. Reitze, J. Richardson, R. Robie, I. Romero-Shaw, R. Route, S. Rowan, R. Schnabel, M. Schneewind, F. Seifert, D. Shaddock, B. Shapiro, D. Shoemaker, A. S. Silva, B. Slagmolen, J. Smith, N. Smith, J. Steinlechner, K. Strain, D. Taira, S. Tait, D. Tanner, Z. Tornasi, C. Torrie, M. V. Veggel, J. Vanheijningen, P. Veitch, A. Wade, G. Wallace, R. Ward, R. Weiss, P. Wessels, B. Willke, H. Yamamoto, M. J. Yap, and C. Zhao, "A cryogenic silicon interferometer for gravitational-wave detection", Classical and Quantum Gravity **37**, 165003 (2020).